Research Article | Vol. 26, No. 19 | 17 Sep 2018 | OPTICS EXPRESS 25166
Optics EXPRESS

# Lyman-β narrowband coatings with strong Lyman-α rejection

LUIS V. RODRÍGUEZ-DE MARCOS,[1,2,3] JUAN I. LARRUQUERT,[1,*] JOSÉ A. MÉNDEZ,[1] MANUELA VIDAL-DASILVA,[1] SERGIO GARCÍA-CORTÉS,[1] NURIA GUTIÉRREZ-LUNA,[1] LUCÍA ESPINOSA-YÁÑEZ,[1] CARLOS HONRADOBENÍTEZ,[1] AND JOSÉ CHAVERO-ROYÁN[1]

[1]*GOLD, Instituto de Óptica-Consejo Superior de Investigaciones Científicas (CSIC) Madrid, Spain*
[2]*Singapore Synchrotron Light Source (SSLS), National University of Singapore (NUS), Singapore*
[3]*slslvrd@nus.edu.sg*
**j.larruquert@csic.es*

**Abstract:** Novel narrowband multilayer coatings efficient at a wavelength as short as 100 mn are presented, which pushes shortwards the existing limit of reported narrowband multilayers. Such limit had been established at ~120 nm, close to the $MgF_2$ cutoff wavelength. The new multilayers combine layers of Al, LiF, and SiC, in an Al/LiF/SiC/LiF multilayer design (four layers, starting with the innermost layer). Among these materials, Al and LiF are deposited by evaporation and SiC by ion-beam-sputtering. In addition to a high, narrow peak close to H Lyman β (102.6 nm), these multilayers simultaneously provide a very small reflectance at H Lyman α (121.6 nm). This combined performance is demanded in space instrumentation for astrophysics and solar physics observations among others, where imaging the sky at the important diagnostic spectral line of Lyman β line requires rejecting the frequently much more intense background at Lyman α line. Such is the case for solar corona observations at Lyman β, which is masked by the strong Lyman α line. The multilayer peak is placed close to another important diagnostic tool: the OVI doublet at 103.2 and 103.8 nm. The target of small reflectance at 121.6 nm was seen to be the most critical. The best strategy in multilayer preparation was to prepare it with such minimum reflectance at slightly shorter wavelengths so that the coating evolved to shift it longwards over time. Multilayers kept a remarkable 102.6 nm/121.6 nm reflectance ratio over time in spite of some performance degradation. Hence, a multilayer coating aged of 4 years kept a reflectance of 43% at 102.6 nm and 0.2% at 121.6 nm.



## 1. Introduction

Observations in the far ultraviolet (FUV, λ<200 nm) down to the H Lyman series limit (91.2 nm) are demanded by the solar physics and astrophysics communities since key spectral lines of basic constituents lie in this range [1]. For gas at temperatures of a few hundred thousand kelvins, intermediate to the temperature regimes sampled by optical and X-ray observations, emission is dominated by transitions of the lithium-like ions such as OVI (103.2 and 103.8 nm), and also longer wavelengths such as NV (123.8 and 124.2 nm) and CIV at 154.8, and 155.0 nm [2]. Emission from non-radiative interstellar shocks, still poorly understood, is dominated by FUV emission, and the brightest emission is OVI doublet [3]. H Lyman β (102.6 nm) and CIII (97.7 nm), along with the O VI doublet, are important atomic tracers relevant to a wide range of astrophysics targets [4]. Mapping the solar chromosphere, transition region and corona relies upon lines such as H Lyman β and OVI. Exoplanetary discovery and characterization, cosmic origins, and planetary science also require imaging and spectroscopy in the short wavelengths of the FUV range; for instance, the proposed space instrument LUMOS includes the use of a filter peaked around 108 nm [5]. Hence, imaging at these spectral lines is expected to reveal valuable and diverse information.

#338554 https://doi.org/10.1364/OE.26.025166
Journal © 2018 Received 24 Jul 2018; revised 26 Aug 2018; accepted 27 Aug 2018; published 12 Sep 2018

Optics EXPRESS

Nowadays, the efficiency of FUV optics limits imaging performance, and the development of narrowband coatings tuned at the aforementioned wavelengths is a key element for the future generation of space instruments. FUV narrowband imaging is difficult to perform due to absorption of materials in nature, particularly below the $MgF_2$ cutoff wavelength at ~115 nm. Hence, the spectral range between 90 and 120 nm lacks of narrowband coatings. For observations of the solar corona, H Lyman β line may be masked by the more intense H Lyman α line, which is the strongest line of the solar spectrum [6,7]. Another unwanted source of H Lyman α light originates at the Earth's atmosphere in the form of geocoronal airglow [8]. Geocoronal H Lyman α line tends to be orders of magnitude brighter than astrophysical FUV emission; hence, any FUV instrument designed to observe wavelengths shorter than 121.6 nm must strongly suppress geocoronal Lyman α [2].

Whilst fully narrowband coatings tuned at the above spectral lines are difficult to make, at least they should meet the requirement of strongly rejecting H Lyman α (121.6 nm). Fortunately, H Lyman β and OVI lines are still on the edge of the transparency range of LiF, the material in nature that extends transparency down to the shortest possible wavelength, what makes LiF the best choice of transparent material for multilayer coatings peaked at 102.6 to 103.8 nm.

No real narrowband performance has been developed for this range other than the combined natural transmittance band of In and LiF, with a relatively modest performance [9]. Outside coatings, other solutions have been proposed, such as the subtraction of two images acquired with edge filters, each with a different short-wavelength cutoff [10,11]. Designs replacing one telescope mirror with a diffraction grating have been proposed to obtain narrowband imaging at H Lyman β or OVI with a rejection of H Lyman α [2,4,7], but the overall performance would be reduced by the limited grating efficiency· Regarding wideband mirrors down to 100 nm, coatings of Al overcoated with LiF, are available with relatively high reflectance at Lyman β and OVI [12–15].

In this research we address the development of narrowband coatings with high reflectance at H Lyman β, which could be extended to also include OVI lines, and at the same time are able to reject Lyman α with a small reflectance at this line. Other than some multilayer designs [16,17], literature reports a pioneering work on this subject published by Edelstein [18]. He performed a preliminary investigation and got to a 3-layer coating with a high 102.6/121.6 nm reflectance ratio, although with no specific narrowband performance. Unfortunately, this attempt has not consolidated yet a technology with enough contrast between H Lyman β or OVI with respect to H Lyman α spectral lines that could be used in space instruments.

At still shorter wavelengths, an analogous two-wavelength photometric performance has been addressed in the literature consisting in the development of coatings with a good 83.4/121.6 nm reflectance ratio, 83.4 nm being an O II line of interest for atmosphere physics [19–21]. In some of these investigations [20], a relatively high reflectance ratio was also obtained between H Lyman β and OVI spectral lines with respect to H Lyman α, although with a modest reflectance at the former. More strictly narrowband coatings peaked below 100 nm have also been proposed [22–24], although without a specific strong rejection at 121.6 nm.

The present research reports narrowband coatings tuned close to H Lyman β with a strong rejection at H Lyman α, based on the material combination of Al, LiF, and SiC. The paper is organized as follows. Section 2 describes the experimental techniques. Section 3 presents various designs based on the combination of Al, LiF, and SiC films and reflectance measurements of fresh and aged multilayers.

## 2. Experimental equipment

Multilayer coatings were deposited and measured in a combined reflectometer and deposition system at GOLD (Spanish acronym for Thin Film Optics Group), which enables in situ

Optics EXPRESS

characterization in the extreme UV (EUV)-FUV of UHV-prepared coatings. In this reflectometer-deposition system, multilayer coatings can be prepared using two different deposition techniques: ion-beam-sputtering (IBS) and evaporation, and both were used in this research. Since the two techniques are in different UHV chambers that are connected in vacuum, the samples travelled without breaking vacuum from the evaporation to the IBS chamber and back in order to alternate evaporation and sputtering in the multilayer. Base pressure in the evaporation and IBS chambers were ~$2 \times 10^{-8}$ and $7 \times 10^{-8}$ Pa, respectively. When the multilayer was completed, we transferred it to the reflectometer without breaking vacuum, so that reflectance could be measured for freshly-deposited coatings.

Al and LiF films were deposited by evaporation. Thermal sources for Al and LiF were W multi-stranded filaments and Mo boats, respectively. The purity of material sources was 99.999% for Al and VUV-grade for LiF. Deposition rate was 0.5-0.9 (Al) and 0.2-0.5 (LiF) nm/s. Films of SiC and C were deposited by IBS, i.e. by impinging energetic ions at 45° on a target placed facing the substrate. 96.5-mm diameter targets were used with a purity of 99.9995% and 99.999% for CVD-SiC and C, respectively. The target was placed in a rotatable target holder that hosts up to four targets, which are cooled down with water. Ions were produced by means of a 3-cm hollow cathode ion gun working with a hollow cathode neutralizer; this gun and neutralizer contain no filament, which minimizes contamination. Typical deposition conditions were ion energy of 1200 eV and total ion current of ~60 mA. Ar was used as a process gas. Chamber pressure increased over the evaporation process up to ~$10^{-6}$ Pa (Al) and ~$2x10^{-7}$ Pa (LiF) and over the sputtering process up to ~$7x10^{-2}$ Pa. Film thickness was measured with a quartz-crystal monitor, which was previously calibrated through Tolansky interferometry. Multilayers were deposited onto 2”x2” size, polished float glass substrates that were not heated or cooled intentionally.

GOLD`s reflectometer was used to measure sample reflectance in the EUV-FUV. The reflectometer has a grazing-incidence, toroidal-grating monochromator, in which the entrance and exit arms are 146° apart. The monochromator covers the 12.5-200 nm spectral range with two Pt-coated diffraction gratings that operate in the long (250 l/mm) or in the short (950 l/mm) spectral range. A windowless discharge lamp was used in this work. The lamp is fed with various pure gases or gas mixtures with which it can generate many spectral lines to cover the spectral range of interest. The beam divergence was ~1.5 mrad and angle accuracy is estimated as ± 0.1°. The sample holder can fit samples up to an area of 50.8x50.8 $mm^2$. A channel electron multiplier with a CsI-coated photocathode was used as the detector. Reflectance was obtained by alternately measuring the incident intensity and the intensity reflected by the sample. The EUV-FUV reflectance of all samples was measured at 5° from the normal incidence; the reflectance of some samples was measured as a function of the incidence angle.

The EUV-FUV reflectance of all samples displayed in this research was first measured in situ, what is referred to as fresh. The samples were later extracted from vacuum and stored in a desiccator, and the FUV reflectance of the aged samples was measured after some storage periods. The desiccator kept an average relative humidity (RH) of less than 30% by means of blue silica gel drying pearls; however the RH might have increased beyond 30% in some periods due to irregular maintenance.

A Lambda-900 Perkin-Elmer double-beam spectrophotometer was used to measure specular reflectance at wavelengths longer than 190 nm with the universal reflectance accessory. Reflectance measurements were performed at a normal angle of 8°. Measurements cannot be made at 5° with this accessory. Anyway, reflectance dependence on incidence angle is small in this angle range for the present multilayers, so that no noticeable difference is expected between 5° and 8°.

Grazing incidence x-ray reflectometry (XRR) measurements were performed at *Centro de Asistencia a la Investigación* (CAI), Universidad Complutense de Madrid (UCM). The diffractometer system was a PANalytical X`pert PRO MRD. A Cu anode under 45 kV

Optics EXPRESS

discharge was used as the source. The Cu Kα (λ = 0.154 nm) line was selected by a graphite monochromator. Measurements were performed at the grazing incident angles from 0.1° to 2°, with a step of 0.005°.

## 3. Results

### *3.1 Coatings with SiC and C outermost layer*

The first attempt consisted in preparing Al/LiF/SiC multilayers (starting with the innermost layer), one layer per material, in the confidence that SiC is a relatively stable material that undergoes a limited oxidation that keeps high EUV reflectance over time, both as a single layer and as the top layer of a multilayer [25]. The reflectance of an Al/LiF/SiC multilayer sample (design D1), both fresh and aged in a desiccator, is plotted in Fig. 1a. Even though this design resulted in fresh coatings with a good performance at the target wavelengths, reflectance evolved negatively over time both at the peak and at 121.6 nm. Particularly reflectance at the latter wavelength was seen to be more critical, with a large increase over time [26]. Layer thicknesses of this and all other multilayers reported in this research are given in Table 1.

**Table 1. Nominal layer thicknesses of the various multilayers designed with high reflectance at 102.6 nm and small reflectance at 121.6 nm[a]**

| Design | Mater. | Thick. | Mater. | Thick. | Mater. | Thick. | Mater. | Thick. | Samples |
|---|---|---|---|---|---|---|---|---|---|
| D1 | Al | 45 | LiF | 10.9 | SiC | 5.0 | | | ALS1,ALS2 |
| D2 | Al | 45 | LiF | 9.2 | SiC | 2.7 | C | 2.0 | ALSC1 |
| D3 | Al | 45 | LiF | 14.5 | SiC | 8.8 | LiF | 15.1 | ALSL1, ALSL2, ALSL3, ALSL4, ALSL5, ALSL6 |

[a]: Layer sequence starts with the innermost layer. Thickness is in nm

In view of the negative behavior of the latter multilayer at 121.6 nm we decided to avoid SiC as the topmost layer material and used a thin film of C to protect the outermost layer of SiC (design D2); a 2-nm thin film was selected [27], and the multilayer was reoptimized. The reflectance of an Al/LiF/SiC/C multilayer sample is plotted in Fig. 1b. Again, the fresh multilayer performed well at the two target wavelengths, but reflectance increased at 121.6 nm even more than for the unprotected multilayer after several days stored under normal air. This behavior was not understood but it was considered negative enough as to not make any further efforts on multilayers protected with a C film [24].

Optics EXPRESS

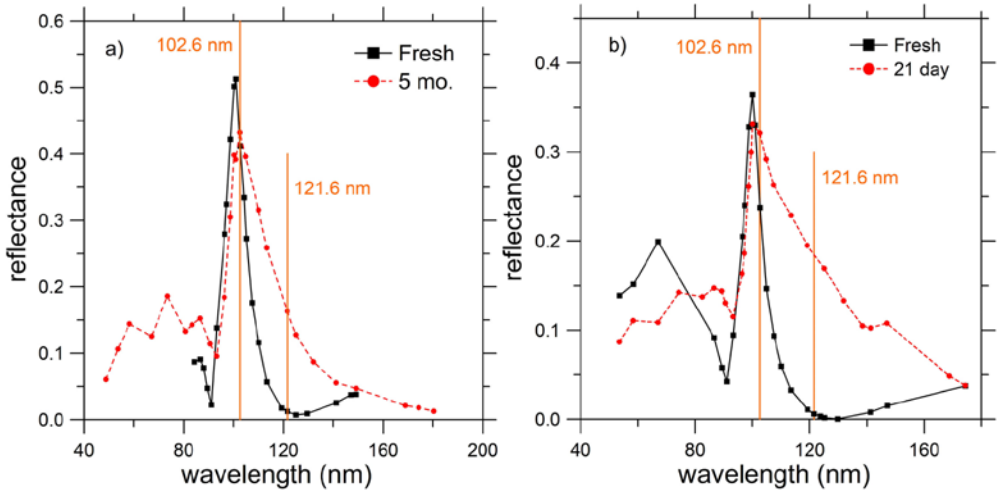


Fig. 1. Near-normal reflectance vs. wavelength of an Al/LiF/SiC multilayer (a: sample ALS1) and of an Al/LiF/SiC/C multilayer (b: sample ALSC1) both fresh and after a period of storage in a desiccator (a) or in air (b). mo: months.

### 3.2 Coatings with LiF outermost layer

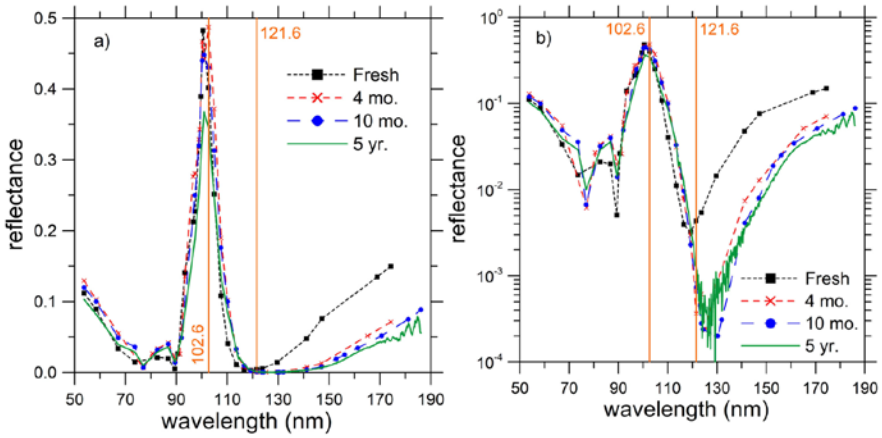


Fig. 2. Near-normal reflectance vs. wavelength of an Al/LiF/SiC/LiF multilayer (sample ALSL1) both fresh and after various storage periods in a desiccator. a: linear axis. b: log axis. mo: months; yr: years.

The next strategy consisted in using a LiF layer to protect the SiC layer. This had not been initially considered because LiF is a material that is somewhat hygroscopic, so that coatings with a LiF outermost layer need to be continuously stored in an environment with a relatively low humidity [28]. However, the shortage of useful materials to make multilayers at 102.6 nm recommended the use of LiF and, in fact, Al mirrors protected with a film of LiF have been used for decades.

Several Al/LiF/SiC/LiF multilayers were prepared with small film thickness differences around design D3 given in Table 1. The 121.6-nm reflectance minimum was observed to be a strong function of small SiC film-thickness variations. For some samples (ALSL1 and ALSL6) we promoted a thickness gradient in the SiC layer by not letting rotate the sample during SiC deposition. In order to quantify the SiC layer thickness gradient, we performed a uniformity scan on sample ALSL1, and from which we estimated a SiC gradient of 17 Å across the sample surface. We took advantage of this SiC thickness gradient by measuring the

Optics EXPRESS

sample at the position with the smallest reflectance at 121.6 nm. We reproduced this strategy when we re-measured each sample, so that measurements plotted in Figs. 2 and 5 do not necessarily correspond to the same sample spot. Contrarily, reflectance at 102.6 nm was found to be approximately independent of the physical locations on the sample.

Figure 2 displays the reflectance of sample ALSL1, both fresh and after various storage periods in a desiccator up to 5 years. The sample kept a peak reflectance of ~45% after 10 months of ageing, but it decreased to ~35% after 5 years. Reflectance at 121.6 nm behaved well over time, since it decreased after 4 months and remained stable up to 5 years, yielding a remarkable 102.6 nm/121.6 nm maximum reflectance ratio of 260 for the 5-year aged sample.

Whatever dynamics affects the multilayer, such as interdiffusion/reaction at the interfaces along with reaction of the outer layer to water vapor, oxygen, etc., such dynamics moved the minimum wavelength of the multilayer displayed in Fig. 2 to cross 121.6 nm and stabilize at ~128 nm and it turned much deeper than for the fresh sample; after a few months, such minimum was rather stable. As for the band, its peak did not essentially shift over time and it was located at ~100 nm, with the performance at 102.6 nm being close to the one at the peak. Regarding peak reflectance, it decayed at a slow speed for months, but it kept decaying over time with an important accumulated decrease after a long ageing period of 5 years. This accumulated decrease may be attributed to that the desiccator humidity was not consistently kept low over such a long period. Such peak-reflectance decrease contrasts with the stability observed at the minimum close to 121.6 nm.

Structural information of design D3 Al/LiF/SiC/LiF multilayers was obtained through XRR. XRR measurements were performed on sample ALSL1 after 11 months of storage in a desiccator. Figure 3 displays XRR measurements, along with the fit, which was performed with IMD software [29]. Table 2 displays the fitting parameters, which were film density, thickness, and RMS roughness (represented as σ).

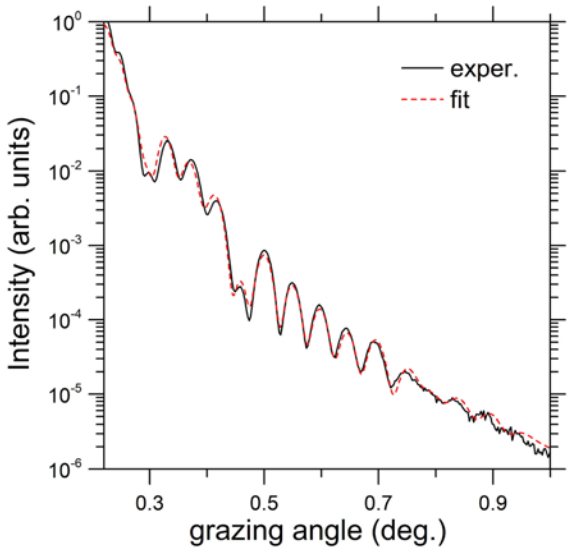


Fig. 3. XRR measurements and fitting data for sample ALSL1 aged of 11 months.

**Table 2. Structural parameters obtained in a fit to XXR measurements for sample ALSL1**

| Material | Thickness (nm) | σ (nm) | Density (g/cm$^3$) |
|---|---|---|---|
| Al | 45 | 2.2 | 2.70 |
| LiF | 16.0 | 2.3 | 2.45 |
| SiC | 8.3 | 2.5 | 2.84 |
| LiF | 14.9 | 2.5 | 2.45 |

Optics EXPRESS

The average density of the LiF layers corresponds to ~82% of the density of the massive material. In the case of SiC, the density value obtained is ~88% of bulk density. Density of Al was not a fitting parameter, and it was fixed to the bulk of 2.7 g / $cm^3$. Regarding roughness, it somewhat increased from bottom to top layers.

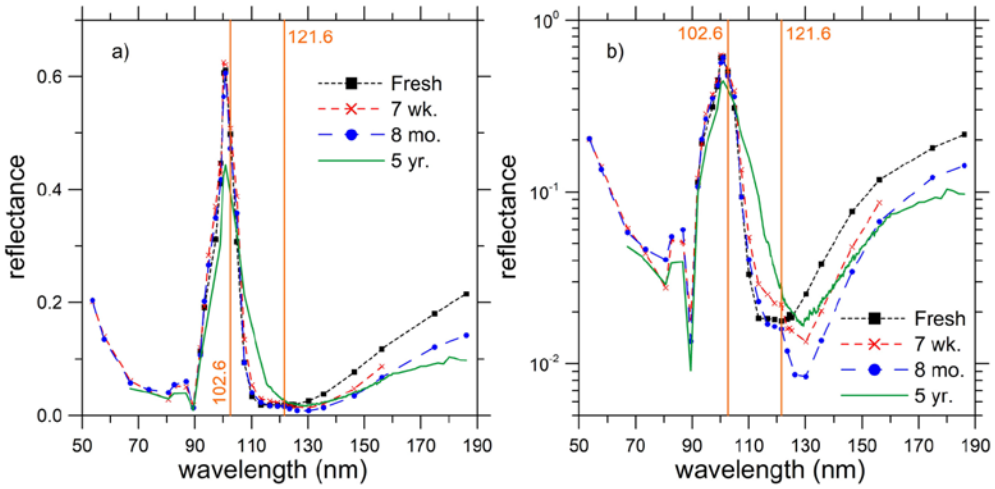


Fig. 4. Near-normal reflectance vs. wavelength of an Al/LiF/SiC/LiF multilayer (sample ALSL5) both fresh and after various storage period in a desiccator. a: linear axis. b: log axis. mo: months; yr: years.

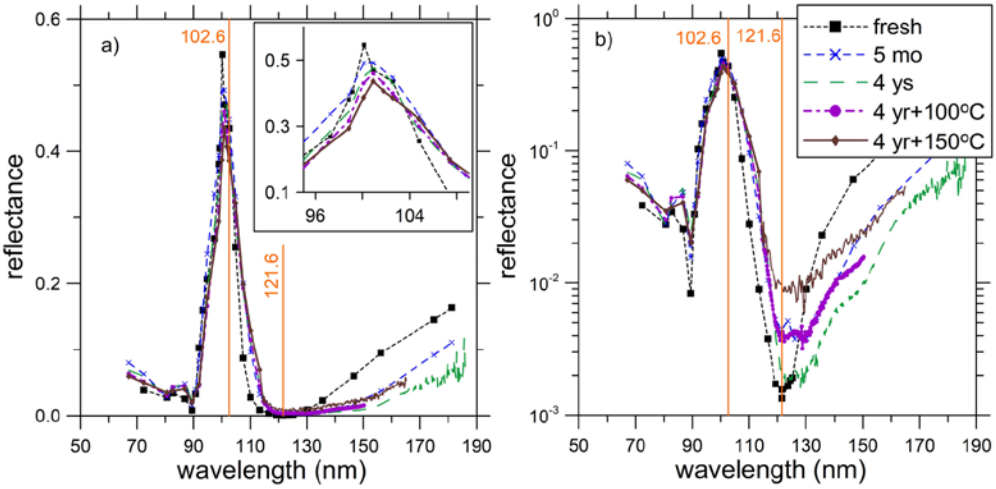


Fig. 5. Near-normal reflectance vs. wavelength of an Al/LiF/SiC/LiF multilayer (sample ALSL6) both fresh and after various storage periods in a desiccator and after two successive annealing processes at the indicated temperature for 1 hour. a: linear axis. b: log axis. mo: months; yr: years.

Other multilayers were prepared with slight film thickness variations to try to better match the target at 121.6 nm, which was seen to be the most critical. This strategy was momentarily successful, in the sense that fresh multilayers with smaller reflectance at 121.6 nm than for the sample plotted in Fig. 2 were measured. However, those multilayers evolved in a more negative way so that their reflectance at 121.6 nm after some months of ageing was not as small as the one displayed in Fig. 2 [30]. The point on this is that the best multilayer is the one that evolves towards the best performance over time.

Optics EXPRESS

Figure 4 displays the reflectance of sample ALSL5. Reflectance was measured both in situ and after various storage periods in a desiccator, up to 5 years. This sample originally had the largest peak reflectance, but also a larger reflectance at 121.6 nm. Peak reflectance was ~60% after an ageing period of 8 months, and underwent an important decrease after a total period of 5 years down to 44%. Reflectance at 121.6 nm behaved positively up to 8 months of ageing, but somewhat increased after 5 years.

Figure 5 displays the reflectance of sample ALSL6. Reflectance was measured both in situ and after 5-month and 4-year storage periods in a desiccator. Peak reflectance decayed from 55% to 47%, which is a less severe decrease than for samples ALSL1 and ALSL5. Ageing resulted in a slight peak shift from ~100.2 to ~100.9 nm. Reflectance at 121.6 nm displayed a more erratic behavior, with an apparent increase after 5 months and an apparent decrease after 4 years. This behavior might be attributed to the selection of a somewhat different sample spot. A 121.6-nm reflectance of 0.2% and a 102.6 nm/121.6 nm ratio of 192 were measured after 4 years of ageing.

After such long ageing period, the previous sample was annealed to evaluate the stability of the multilayer with temperature and also to try to recuperate a higher peak reflectance by evaporating possible condensed contaminants. First annealing at 100°C for 1 hour resulted in some performance decrease, but the coating kept a peak reflectance of 45.7% and a reflectance at 121.6 nm of 0.4%. A further annealing at 150°C for 1 hour resulted in an additional peak reflectance decrease down to 43.5% with a reflectance increase at 121.6 nm to ~1%, still keeping a 102.6/121.6 reflectance ratio of ~38. Hence, even though there was a negative evolution with temperature, the multilayer retained valuable properties of reflecting 102.6 nm and rejecting 121.6 nm. Heating did not produce a further peak shift, although there was some peak shape modification towards increasing reflectance in the long-wavelength descent.

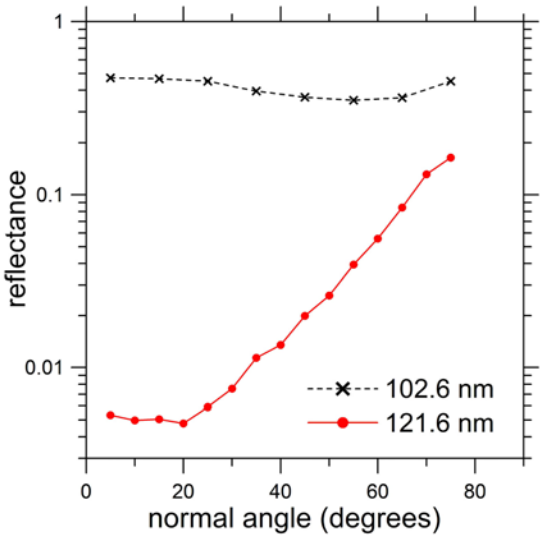


Fig. 6. Reflectance (log axis) vs. normal-incidence angle at the indicated wavelengths of an Al/LiF/SiC/LiF multilayer (sample ALSL6) stored for five months in a desiccator.

Reflectance at 102.6 and 121.6 nm was measured as a function of incidence angle for an Al/LiF/SiC/LiF multilayer sample after a storage period of 5 months in a desiccator and it is displayed in Fig. 6. The reflectometer provides radiation that is partially polarized. The estimate is that partial polarization at the measured wavelengths was $P = (I_p-I_s)/(I_p + I_s) = -0.3$, where $I_p$ and $I_s$ represent the fraction of the radiation intensity impinging on the sample with the electric vector parallel and perpendicular, respectively, to the plane of incidence.

Optics EXPRESS

P<0 stands for a beam with a larger component of s than of p polarization. Reflectance at 102.6 and 121.6 nm had a negligible dependence with angle up to 20° and 121.6-nm reflectance started increasing at larger angles. Reflectance was below 0.01 and above 0.4 up to 30° at Lyman α and β, respectively.

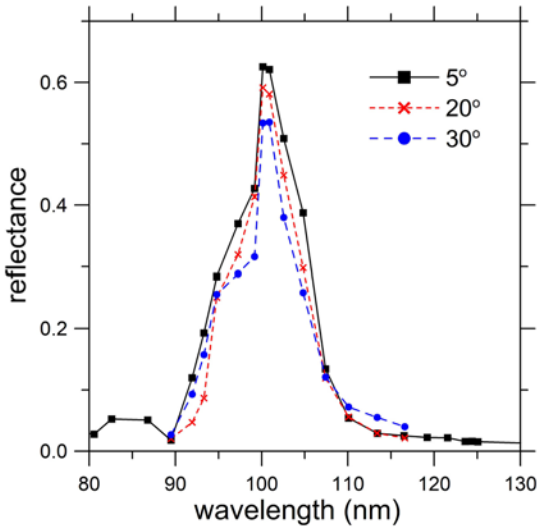


Figure 7. Reflectance vs. wavelength at various normal-incidence angles of an Al/LiF/SiC/LiF multilayer (sample ALSL5) stored for one month in a desiccator.

Reflectance versus wavelength was measured at various angles for an Al/LiF/SiC/LiF multilayer sample after a storage period of 8 months in a desiccator and it is displayed in Fig. 7. The same estimate of partial polarization is applied here. There is a small decrease in performance up to 20° and the decrease is still moderate at 30°, but the narrow band shape remains.

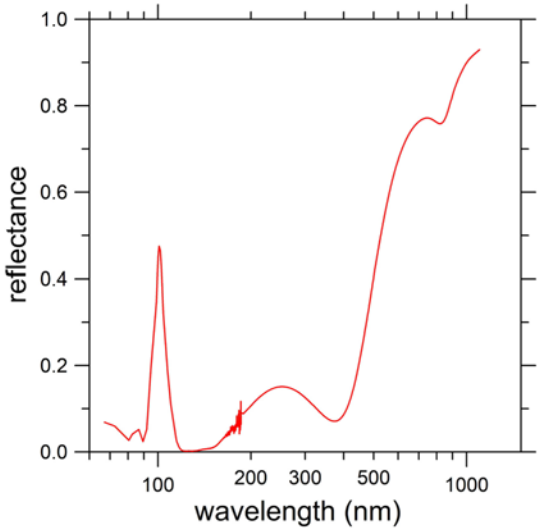


Fig. 8. Near-normal reflectance vs. wavelength extended to the near IR of an Al/LiF/SiC/LiF multilayer (sample ALSL6) after four years of storage in a desiccator.

Sample ALSL6 was measured at longer wavelengths up to the near infrared (NIR). Measurements were performed after 4 years of ageing and before annealing. The full

Optics EXPRESS

spectrum is plotted in Fig. 8. In the out-of-band, reflectance increased with wavelength up to 15% at 253 nm, later decreased down to 7% at 374 nm and then reflectance strongly increased through the visible and displayed high reflectance in the NIR. The latter increase through the visible resulted in a characteristic yellowish interferential color.

Regarding practical applications in space instrumentation, the present coatings are optimal for instruments with solar blind detectors, more specifically, with MCP detectors employing KBr or CsI photocathodes, which are used on many space missions. On the other hand, coating throughput in the near UV and visible would be challenging to filter out if combined with silicon-based detectors.

## Conclusions

Narrowband multilayer coatings peaked at a wavelength as short as 100 nm have been developed. The multilayer is based on the combination of films of three materials: Al, LiF, and SiC. The narrowband multilayers have been developed with the further requirement of a very small reflectance in a band containing H Lyman α line (121.6 nm). Multilayer performance is effective for space observations at the H Lyman β spectral line (102.6 nm) with a strong rejection of the usually more intense background radiation at H Lyman α line. Multilayers were attempted in which the outermost layer was SiC and also C; those multilayers had a good performance when measured in situ but performance strongly degraded after few weeks or months of storage, mostly because reflectance at 121.6 mn increased over time. Multilayers with LiF as the outermost layer resulted in a remarkable performance both in situ and after storage in a desiccator for many months. A multilayer coating aged of 11 months in a desiccator retained a peak reflectance of 45% at ~100 nm with a reflectance below 0.1% at 121.6 nm. A largest peak reflectance of 60% was obtained for an 8-month old multilayer with slight film thickness difference compared to the first design. Multilayer reflectance kept relatively small at longer wavelengths up to ~400 nm, where a steep increase was observed through the visible. Peak reflectance and antireflection at 121.6 nm were not strongly dependent on the angle of incidence, with small variations up to an angle of ~30°.

A further storage period of 4 to 5 years in a desiccator resulted in a more severe reflectance loss at the peak, although the multilayer profile was still efficient at reflecting 102.6 nm and rejecting 121.6 nm. A 121.6-nm reflectance of 0.2% and a 102.6 nm/121.6 nm ratio of 192 were measured for a multilayer after 4 years of ageing. The further peak-reflectance decrease was attributed in part to the fact that the desiccator may not have had a consistent low humidity all over this long period. Further efforts should be made on future coatings to keep them under a consistently low humidity, such as by storing them in a dry nitrogen environment and by handling them under a controlled low humidity.

A multilayer sample that had been stored for 4 years in a desiccator was annealed to 100°C for 1 hour; it underwent some performance decrease, but it retained a peak reflectance of 45.7% with a 0.4% reflectance at 121.6 nm. After a further 1-h annealing at 150°C the multilayer retained a peak reflectance of 43.5% and a reflectance at 121.6 nm of 1%, keeping a 102.6/121.6-nm reflectance ratio of 38.

## Funding

Spanish Programa Estatal de Investigación Científica y Técnica de Excelencia, Secretaría de Estado de Investigación, Desarrollo e Innovación (AYA2013-42590-P, ESP2016-76591-P).

## Acknowledgments

We are indebted to J. Campos, A. Pons, and J. L. Bris for spectrophotometer measurements, and to I. Carabias and “Centro de Asistencia a la Investigación”, Universidad Complutense de Madrid (UCM), for grazing incidence x-ray reflectometry measurements.

Optics EXPRESS

## References


1. K. Sembach, "Technology investments to meet the needs of astronomy at ultraviolet wavelengths in the 21st Century," Astro2010 Technology Development White Paper, 2010. Available at *https://www.astro.princeton.edu/~dns/Theia/Sembach_UVtechnology_EOS.pdf*
2. N. J. Cunningham and E. Wilkinson, "Holographic telescope design for wide field imaging of O VI 1032, 1038 Å," Proc. SPIE **5166**, 296–306 (2004).
3. M. Beasley, C. Boone, N. Cunningham, J. Green, and E. Wilkinson, "Imaging spectrograph for interstellar shocks: a narrowband imaging payload for the far ultraviolet," Appl. Opt. **43**(24), 4633–4642 (2004).
4. J. C. Green and K. France, "SubLymE: The Sub-Lyman α Explorer," Proc. SPIE **9144**, 914405 (2014).
5. K. France, B. Fleming, G. West, S. R. McCandliss, M. R. Bolcar, W. Harris, L. Moustakas, J. M. O'Meara, I. Pascucci, J. Rigby, D. Schiminovich, and J. Tumlinson, "The LUVOIR Ultraviolet Multi-Object Spectrograph (LUMOS): Instrument definition and design," Proc. SPIE **10397**, 1039713 (2017).
6. A. Vourlidas, B. S. Andrade-Nuño, E. Landi, S. Patsourakos, L. Teriaca, U. Schühle, C. M. Korendyke, and I. Nestoras, "The structure and dynamics of the upper chromosphere and lower transition region as revealed by the subarcsecond VAULT observations," Sol. Phys. **261**(1), 53–75 (2010).
7. P. Lemaire, J. C. Vial, W. Curdt, U. Schüble, and T. N. Woods, "The solar hydrogen Lyman α to Lyman β line ratio," Astron. Astrophys. **542**, L25 (2012).
8. E. Wilkinson, R. Indebetouw, and M. Beasley, "Technique for narrow-band imaging in the far ultraviolet based on aberration-corrected holographic gratings," Appl. Opt. **40**(19), 3244–3255 (2001).
9. G. R. Carruthers, "Narrow-Band filters for the Lyman β wavelength region," Appl. Opt. **10**(6), 1461–1463 (1971).
10. H. Ford, F. Bartko, P. Bely, T. Broadhurst, C. Burrows, E. Cheng, M. Clampin, J. Crocker, P. Feldman, D. Golimowki, G. Hartig, G. Illingworth, R. Kimble, M. Lesser, G. Miley, S. Neff, M. Postman, W. Sparks, Z. Tsvetanov, R. White, P. Sullivan, C. Krebs, D. Leviton, T. LaJeunesse, B. Burmester, S. Fike, R. Johnson, B. Slusher, P. Volmer, and B. Woodruff, "The Advanced Camera for the Hubble Space Telescope," Proc. SPIE **3356**, 234–248 (1998).
11. J. I. Larruquert, J. A. Méndez, J. A. Aznárez, M. Vidal-Dasilva, S. García-Cortés, L. Rodríguez-de Marcos, and M. Fernández-Perea, "GOLD's coating and testing facilities for ISSIS-WSO," Astrophys. Space Sci. **335**(1), 305–309 (2011).
12. J. T. Cox, G. Hass, and J. E. Waylonis, "Further studies on LiF-overcoated Aluminum mirrors with highest reflectance in the vacuum ultraviolet," Appl. Opt. **7**(8), 1535–1540 (1968).
13. W. R. Hunter, J. F. Osantowski, and G. Hass, "Reflectance of Aluminum overcoated with $MgF_2$ and LiF in the wavelength region from 1600 Å to 300 Å at various angles of incidence," Appl. Opt. **10**(3), 540–544 (1971).
14. M. R. Adriaens and B. Feuerbacher, "Improved LiF and $MgF_2$ overcoated Aluminum mirrors for vacuum ultraviolet astronomy," Appl. Opt. **10**(4), 958–959 (1971).
15. B. Fleming, M. Quijada, J. Hennessy, A. Egan, J. Del Hoyo, B. A. Hicks, J. Wiley, N. Kruczek, N. Erickson, and K. France, "Advanced environmentally resistant Lithium Fluoride mirror coatings for the next generation of broadband space observatories," Appl. Opt. **56**(36), 9941–9950 (2017).
16. G. L. Keller, M. L. Scott, and K. Mitchell, "Performance of oblique angle of incidence collection systems in the VUV," Proc. SPIE **689**, 231–237 (1986).
17. P. Conconi, G. Pareschi, E. Antonello, S. Scuderi, and L. Poletto, "Multilayer coatings for the Ultraviolet Italian Sky Surveyor (UVISS) on the International Space Station," Proc. SPIE **4854**, 397–404 (2003).
18. J. Edelstein, "Reflection/ suppression coatings for the 900–1200 Å radiation," Proc. SPIE **1160**, 19–25 (1989).
19. J. F. Seely and W. R. Hunter, "Thin film interference optics for imaging the O II 834-Å airglow," Appl. Opt. **30**(19), 2788–2794 (1991).
20. S. Chakrabarti, J. Edelstein, R. A. M. Keski-Kuha, and F. T. Threat, "Reflective coating of 834 Å for imaging $O^+$ ions," Opt. Eng. **33**(2), 409–413 (1994).
21. J. I. Larruquert and R. A. M. Keski-Kuha, "Multilayer coatings for narrow-band imaging in the extreme ultraviolet," Appl. Opt. **40**(7), 1126–1131 (2001).
22. M. Vidal-Dasilva, M. Fernández-Perea, J. A. Méndez, J. A. Aznárez, and J. I. Larruquert, "Narrowband multilayer coatings for the extreme ultraviolet range of 50-92 nm," Opt. Express **17**(25), 22773–22784 (2009).
23. J. I. Larruquert, M. Vidal-Dasilva, S. García-Cortés, L. Rodríguez-de Marcos, M. Fernández-Perea, J. A. Aznárez, and J. A. Méndez, "Multilayer coatings for the far and extreme ultraviolet," Proc. SPIE **8076**, 80760D (2011).
24. M. Fernández-Perea, R. Soufli, J. C. Robinson, L. Rodríguez-De Marcos, J. A. Méndez, J. I. Larruquert, and E. M. Gullikson, "Triple-wavelength, narrowband Mg/SiC multilayers with corrosion barriers and high peak reflectance in the 25-80 nm wavelength region," Opt. Express **20**(21), 24018–24029 (2012).
25. J. I. Larruquert and R. A. M. Keski-Kuha, "Multilayer coatings with high reflectance in the extreme-ultraviolet spectral range of 50 to 121.6 nm," Appl. Opt. **38**(7), 1231–1236 (1999).
26. J. I. Larruquert, J. A. Méndez, J. A. Aznárez, M. Vidal-Dasilva, and S. García-Cortés, "Coatings with high 102.6-to-121.6 nm reflectance ratio," Proc. SPIE **8443**, 84433P (2012).
27. J. I. Larruquert and R. A. M. Keski-Kuha, "Multilayer coatings for narrow-band imaging in the extreme ultraviolet," Appl. Opt. **40**(7), 1126–1131 (2001).

Optics EXPRESS

28. C. M. Oliveira, K. Retherford, S. J. Conard, R. H. Barkhouser, and S. D. Friedman, "Aging studies of LiF-coated optics for use in the far ultraviolet," Proc. SPIE **3765**, 52–60 (1999).
29. D. L. Windt, "IMD - Software for modeling the optical properties of multilayer films," J. Comput. Phys. **12**(4), 360–370 (1998).
30. L. Rodríguez-de Marcos, J. I. Larruquert, J. A. Méndez, J. A. Aznárez, M. Vidal-Dasilva, and L. Fu, "Narrowband filters for the FUV range," Proc. SPIE **9144**, 91440Y (2014).